Evaporation in a single channel in the presence of particles

Elisa Ghiringhelli, Manuel Marcoux, Sandrine Geoffroy, Marc Prat

Version of Record: https://www.sciencedirect.com/science/article/pii/S0927775722021872
Manuscript_db99f371ebf0ad174d3a79babf559570

Evaporation in a single channel in the presence of particles

Elisa Ghiringhelli[a], Manuel Marcoux[a], Sandrine Geoffroy[b], Marc Prat[a*]

[a]Institut de Mécanique des Fluides de Toulouse (IMFT), Université de Toulouse, CNRS – Toulouse, France

[b]LMDC (Laboratoire Matériaux et Durabilité des Constructions), Université de Toulouse, INSAT, UPS, France

*corresponding author: mprat@imft.fr

Abstract:

Liquid corner films in channels or pores of polygonal cross-section are known to have a strong impact on evaporation with a much faster evaporation compared to a tube of circular cross section. The aim of this work is to study the interplay between colloidal particles, development of the corner films and evaporation in a micro channel from a combination of visualization experiments with fluorescent particles and numerical simulations. It is shown that the triple line pinning along the corner films due to particle accumulation in the films leads to the thinning of the corner films. As a result of the film thinning, evaporation is slower in the presence of particles compared to pure water. The identification of such an evaporation reduction mechanism at pore scale shed new light on the phenomenon of reduced evaporation in porous media due to the presence of colloidal particles reported in previous works.

Key words: colloidal suspension, evaporation, corner liquid films, microchannel, wettability

1. Introduction

Drying of colloidal dispersions has been the subject of many studies, e.g. [1-2] and references therein, because it is both a fascinating phenomenon and of importance as a common industrial process as well as for engineering innovative materials [3]. As pointed out in [4], drying of a suspension in a porous medium is also frequent in industry and nature in relation with the transport of pollutants through soils [5], the evolutions of soil fertility [6], the hydrophobization of porous components [7] or the improvement of the thermal properties of electronic chips [8], to name only a few. Nevertheless, the understanding and modeling of the effect of colloidal suspensions in a drying porous medium are less advanced than for the

drying of suspensions, e.g. [10] and references therein, but have significantly been improved in recent years thanks to new experimental and numerical studies, e.g. [4], [10], [11], [12]. In [12], the focus was on the formation of clogging structures induced by evaporation within a model porous medium from numerical simulations at the pore scale. In [4] and [11], experimental results with granular medium columns showed that drying is slower in the presence of particles compared to pure water. The greater the particle concentration, the slower is the drying. As in the case of drying with a saline solution, e.g. [13], [14], the particles are transported by advection up to the evaporative surface where they accumulate, deposit and reduce the porosity [12]. This process leads to the formation of a region with deposited particles on top of the granular column [4]. The gradual decrease of the evaporation rate was then explained by the formation of a receding evaporation front into the medium as a result of the deposit of particles in the top region of the column.

On the other hand, it has been shown that thick capillary liquid films, also referred to as corner liquid films, can have an important impact in drying, e.g. [15-18]. These films form in crevices or corners in the pore space are distinct from the thin films with thickness of the order of nanometers, e.g. [19]. Compared to that of thick capillary films, the contribution of thin films to the overall liquid flow in drying is considered as negligible [16]. In the simple situation of evaporation in a capillary tube, drying is much faster in a square tube compared to drying in a circular tube due to the presence of capillary liquid films along the inner corners of the square tube. Such an enhanced evaporation effect was also reported in micromodel experiments [20] as well as in a packing of grains confined between two plates [18]. Thus, the question arises as to whether a slower drying in the presence of particles can be attributed to the effect of particles on the capillary films. In this article, this question is addressed from evaporation experiments in a channel of almost square cross-section in conjunction with numerical simulations combining Surface Evolver [21] simulations of the gas-liquid interface in the channel and computations of the evaporation rate using a commercial code.

The paper is organized as follows. The materials and methods are presented in Section 2. Experimental results are presented and analyzed in Section 3 with the help of numerical simulations. The influence of corner film thickness on evaporation rate is determined in Section 4 from numerical simulations. Section 5 consists of the main conclusions of the study.

2. Materials and methods

Evaporation experiments are conducted in a channel of rectangular cross section. The channel is 2.4 mm long, with a width of 0.8 mm and a depth of 1mm. As illustrated in Fig.1,

this is a composite channel with four walls made of a hydrophilic material (SUEX^{TM}), namely the end wall, lateral walls and bottom wall, whereas the top wall is in polydimethylsiloxane (PDMS). This composite feature facilitates the observation of corner films, which, as it will be shown, develop only along the two lower corners of the channel. The channel is crafted using UV lithography of 1mm SUEX epoxy film. The microfabrication sequence is the following: a glass plate used as support, is cleaned with acetone, ethanol and dried with compressed air. The SUEX sheet is set on a hot plate to be cut. Then a first layer of SUEX is set on the glass plate and exposed to UV and stick to the first layer by hot plate heating. A second layer of SUEX is placed on top of it. This resin sheet assembly is put in the UV lamp, covered with the mask imposing the channel shape, to be exposed for 4 minutes at 100% power. To finish, the sheet is developed with propylene glycol methyl ether acetate (PGMEA), cleaned with isopropyl alcohol (IPA) and dried in an oven several hours. This yields a 1 mm deep channel on top of the SUEX sheet assembly. The chip so obtained undergoes a final cleaning protocol. It is gently brushed with soap, rinsed with ethanol and dried with compressed air, in order to remove any residual deposited particles or dust. As illustrated in Fig.1, the developed SUEX chip is covered with a thin layer of PDMS (Fig. 1) to close the channel, ensure proper sealing and avoid leaks.

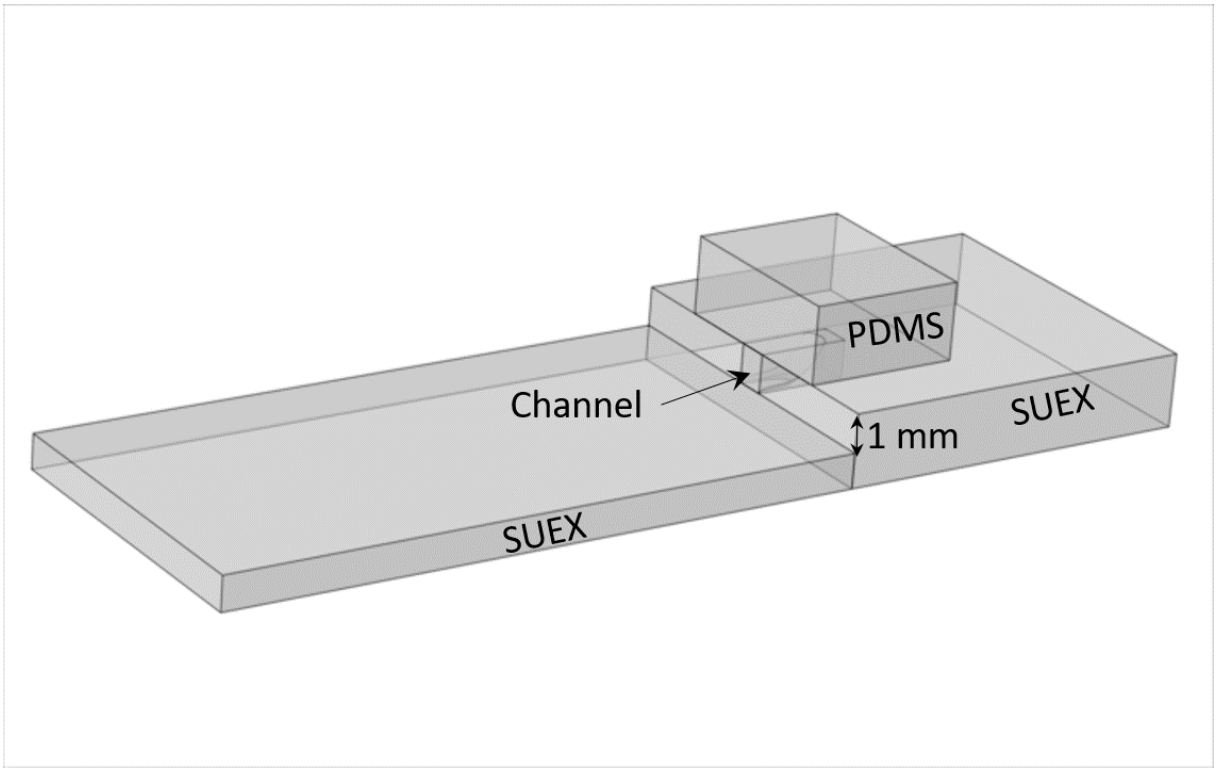

Fig. 1. Composite SUEX -PDMS channel of rectangular cross section.

Evaporation experiments were performed by filling the channel with either pure water or water with particles. The particles were carboxylate-modified fluorescent microspheres of 1 μm in diameter (Molecular Probes^{TM} Fluo 3, maximum absorption 580 nm and emission around 605 nm, density of 1.05 g/mL) available in a solution of distilled water containing particles at a concentration of 2% (g/mL). A calibration curve was built to relate the light intensity and the particle concentration using a 16-bit grayscale.

Experiments were carried out as follow. After cleaning the channel and closing it with PDMS, the liquid was injected manually with a syringe. Care was exercised for not flooding the channel so as to avoid any spreading of solution in excess in the outer region of channel. The result was that the channel was not fully filled when the experiment started. Then, the chip was placed under a microscope (Zeiss Axio Scope.A1 with a 5x/0.16Ph1 lens) equipped with a camera (LaVision Image sCMOS) and images of channel during evaporation were taken from the top at a frequency of 0.1Hz. Positions of the triple line on the SUEX bottom wall or PDMS top wall were obtained after image processing using ImageJ and Matlab.

Four experiments, with pure water and three different particles concentrations (in g/mL), namely 10^{-5}, 0.5×10^{-4} and 10^{-4}, were performed. These concentrations were obtained by mixing a volume V_{part} of the 2% (g/mL) solution with a selected volume V_{H2O} of pure water. This gives $C = \frac{Vpart\, C_0}{V_{H2O}+Vpart}$ where C_0 = 0.02 g/mL and C denotes the obtained concentration. Prior to each experiment, the conditions in the box around the microscope were measured and, if necessary, modified with the addition of a salty solution in order to impose the same relative humidity, 58% ± 2% in each experiment. The room temperature was T = 22 ± 1 °C. Both the temperature and relative humidity were recorded every 5 minutes.

The wettability properties of the channel materials were characterized from contact angle measurements. These measurements were performed for pure water and the various concentrations in particles using the Drop Shape Analyzer Krüss based on the sessile drop technique. For both pure water and with particles the contact angle was found to be on the order 70-75° on a SUEX layer. These values correspond to measurements right after the droplet has reached an equilibrium on the SUEX, i.e. a short time after the drop is set on the SUEX plate surface. These values change during the gradual evaporation of the droplet. As can be seen from Fig.2, the contact angle θ of a specific drop during evaporation decreases almost linearly as a function of time for both pure water and water with particles while the triple line remains pinned. The variation is quite significant with the contact angle reaching values less than 20°. While SUEX is a hydrophilic material (θ < 90°), contact angle

measurements on PDMS led to a mean value of 104°, consistent with values in the literature [22], with a limited effect of the particles. However, with the evaporation, the measured contact angle decreases and can become as low as 45-50° (Fig.2), in line with the results reported in [23].

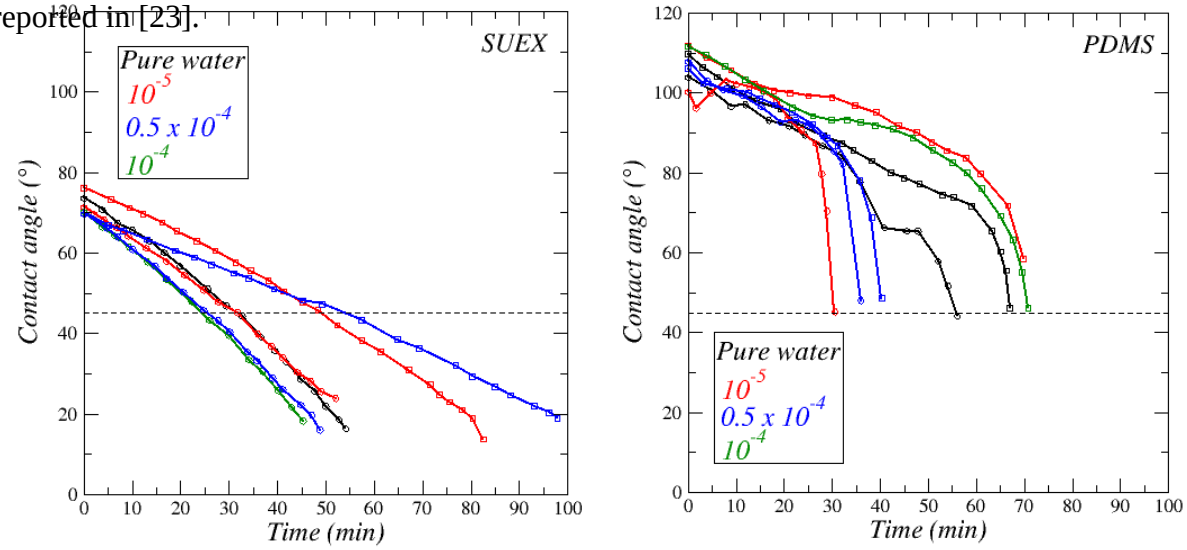

Fig. 2. Contact angle variation on SUEX and PDMS during evaporation of a droplet in the fixed triple line regime for pure water and the three concentrations in particles.

Contact angle measurements were also attempted on particles forming a homogeneous deposit on a SUEX plate. Droplets on the particles deposit spread rapidly leading to the conclusion that the contact angle is close to zero. Hence, the particles are considered as hydrophilic, consistently with a previous work [24], where a contact angle value of 34° is indicated for carboxylate modified polystyrene particles.

As indicated in the introduction, numerical simulations were also performed using the open-source software "Surface Evolver" [21]. This software allows computing the quasi-static liquid-gas interface within the channel, i.e. the shape of the interface when capillary effects are dominant. The parameter which is varied in these simulations is the saturation. A given volume fraction S_ℓ of liquid is set in the channel under the form of a plug almost filling the channel from its end. Then the plug shape in the channel evolves in the simulation due to capillary effects until the equilibrium shape is reached. The next step is to gradually reduced the liquid volume (which is an imposed constraint in the Surface Evolver simulations). A new equilibrium shape is obtained for each considered liquid volume. Hence, by decreasing S_ℓ (or equivalently by increasing the gas volume fraction S_g), the evolution of the liquid- gas distribution due to the evaporation process is mimicked. As explained in Section 4, some of the liquid gas distributions computed with Surface Evolver were also used to compute the

evaporation rate by importing the Surface Evolver computed interface shapes in the commercial code COMSOL Multiphysics.

3. Results

3.1 Phase distribution

The typical liquid distribution in the composite channel during evaporation is illustrated in Fig.3a for pure water. A main meniscus, also referred to as the bulk meniscus, forms within the channel. This meniscus is attached to the top wall (in PDMS) and to the bottom wall (in SUEX). As can be seen, the difference in wettability between PDMS and SUEX introduces a distortion in the bulk meniscus shape. The triple line is more advanced within the channel on the top wall (PDMS) than on the bottom wall (SUEX). A major feature is also the development of corner liquid films in the lower corners of the channel corresponding to SUEX corners.

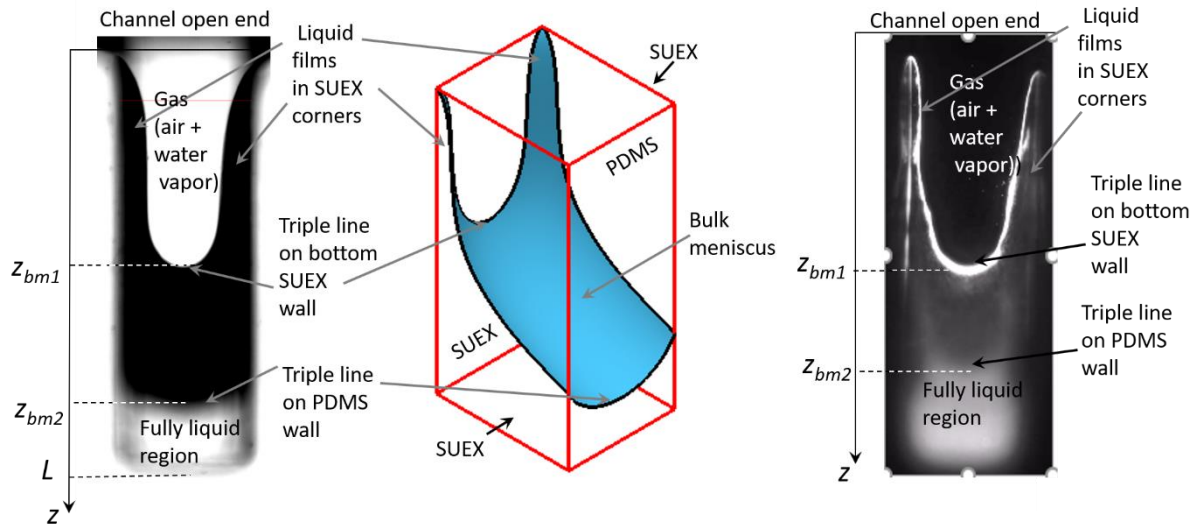

a) b) c)

Fig. 3. Typical fluid distribution in the channel during evaporation: a) top view of the channel in the experiment with pure water, b) quasi-static shape computed with Surface Evolver for θ_{SUEX} = 30° and θ_{PDMS} = 104 °, c) in the presence or particles (C = 10^{-4} g/mL)

Corner films are a well identified feature of evaporation or drainage in tube or channel of polygonal cross-section, e.g. [15, 17, 25, 26]. However, for such films to form, the contact angle must be lower than 45° in the case of a right corner geometry, e.g. [17, 27]. The contact angle fresh value of ~70° (Fig.2, time zero) is not compatible with the development of corner films. As in the case of the droplet evaporation where, as depicted in Fig.2, the contact angle

decreases with time, the contact angle actually decreases and eventually becomes sufficiently small for the corner films to form. From the overlay of the experimental image with the corresponding images obtained from Surface Evolver simulations for various values of the contact angle on the SUEX walls, it is found that the contact angle in the experiment with pure water is $\theta_{SUEX} \approx 30$ °(Fig.4). This value gives a comparable film thickness and a comparable distance difference $z_{bm2} - z_{bm1}$ (Fig.3) between the triple line position on the top PDMS wall and SUEX bottom wall. It can be noted that contact angles below 45° on a SUEX plate are reached after about 30 minutes in the contact angle measurements reported in Fig.2. However, no delay in the corner film formation is noticeable in the channel experiments. The corner films form in the channel right from the beginning of the experiments. Why this is so remains to be explained. Perhaps this is due to wall roughness generated on the channel walls during the channel fabrication process.

Since from previous works on evaporation in square tubes, e.g. [15, 28], it is known that the evaporation rate, and thus the bulk meniscus displacement speed, highly depends on the corner liquid films, it is interesting to look at the effect of particles on the corner films.

The comparison of the triple line on the SUEX bottom plate for various concentrations in particles in Fig.5 shows that the particle presence significantly affects the corner films (as evidenced by the comparison with the shape in yellow which corresponds to the pure water case). Whereas the corner film shape is typical of a quasi-static shape in the case of pure water (the film thickness w_{film}, defined at the distance between the triple line and the nearest channel lateral wall in Fig. 5, tends to a plateau at some distance below the channel entrance), the corner films are globally thinner and with a more complex film thickness variations along the channel in the presence of particles (Fig.5).

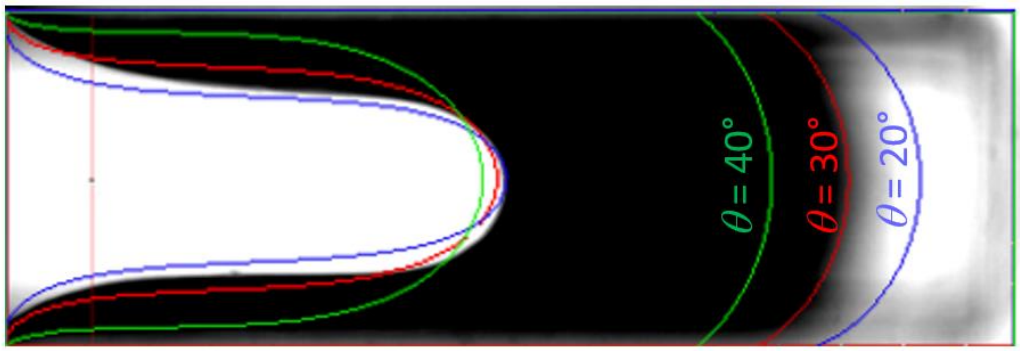

Fig.4. Overlay of picture of the experiment with pure water with focus on the SUEX bottom wall and corresponding images obtained from Surface Evolver simulations (solid lines in

color) for three values of contact angle.

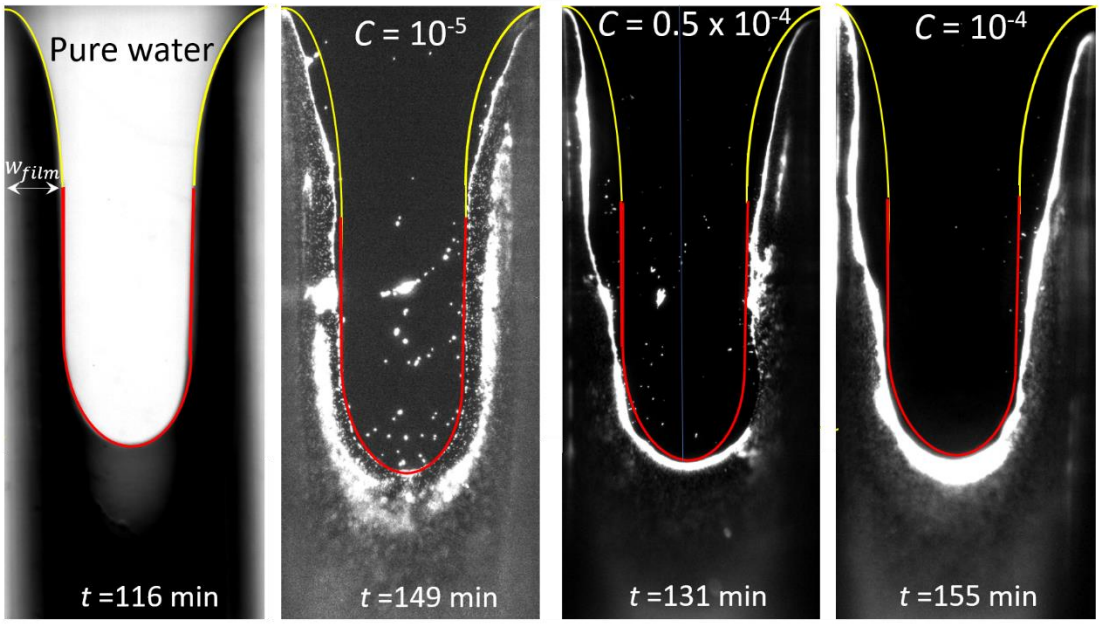

Fig.5. Triple line shape on SUEX bottom plate for pure water and the three particle concentrations. The curve in red is the shape in the main meniscus region in the pure water experiment whereas the shape in yellow is the shape in the corner film upper region in the pure water experiment. The bright zones in the pictures with particles correspond to particle accumulation zones. The indicated times correspond to the time in Fig.8a (see Section 3.2).

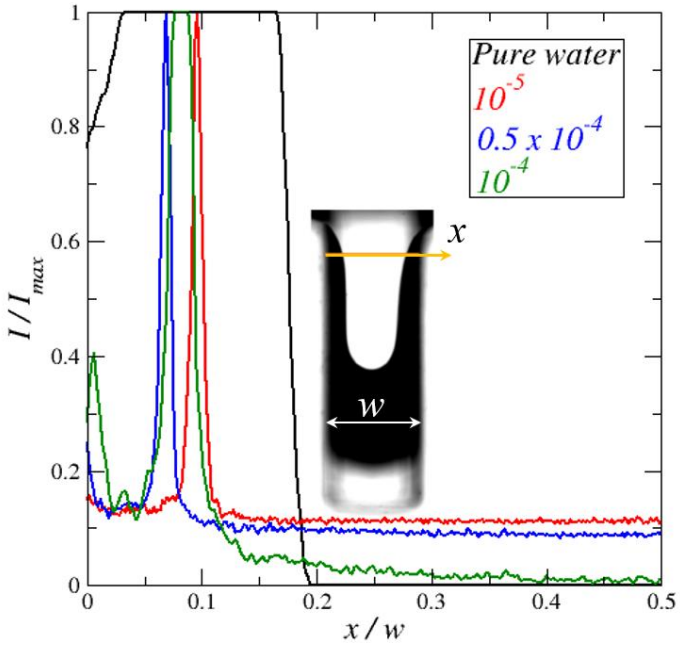

Fig. 6. Corner film thickness at time t = 90 min evaluated at a distance of 0.3 mm from the channel entrance (this location corresponds to the horizontal orange line in the inset); I denotes the light intensity (expressed in grey level in the images). In the images with particles, the light intensity is maximum at the triple line. Note that the plots are over the half

of the channel width.

This is quantified in Fig.6 which shows the liquid-gas distribution over the half of the channel width along a line located at a distance of 0.3 mm from the channel open end (this line is shown in orange in Figs.3a, 4 and 6). Fig.5 shows also the preferential accumulation of particles along the triple line, notably in the corner film region. Nevertheless, as indicated by the shape in red in Fig.5, the triple line shape is somewhat similar in the four experiments in the region of the triple line most advanced points (these correspond to the positions z_{bm1} and z_{bm2} in Fig. 3).

The effect of particles on the corner films is further discussed in Section 5 after presentation of the evaporation kinetics (next two sections) and the particle final deposit.

3.2 Evaporation kinetics (pure water)

The evaporation kinetics in the pure water experiment is illustrated in Figs. 7a and 7b showing the evolution of the triple line most advanced points z_{bm1} and z_{bm2} on the channel SUEX bottom surface and PDMS top surface, respectively and in Figs. 7c and 7d showing the variation of the distance $z_{bm1} - z_{bm2}$.

Three main periods can be distinguished. In the first period the triple line moves faster on the PDMS wall than on the SUEX bottom wall until the quasi-static equilibrium shape illustrated in Fig.3b is reached. The distance between the triple line most advanced point on the PDMS wall and the SUEX bottom wall thus increases in this period (Fig.7c) until a plateau is reached. The plateau in Fig.7c corresponds to the second period where the triple lines move at the same pace on the top and bottom walls (as well as on the lateral walls). In other words, the quasi-static liquid - gas interfacial shape illustrated in Fig.3b moves inward at a constant speed without significant deformation in this second period. The triple line constant speed is also evidenced by the quasi-linear displacement of the triple line most advanced points z_{bm1} and z_{bm2} in Fig.7a.

The third period starts when the triple line on the PDMS wall reaches the end wall. Then the triple line continues moving on the SUEX bottom wall as the mass of liquid confined in the end region of the channel gradually decreases. This is illustrated in Fig.7c, where the distance $z_{bm2} - z_{bm1}$ becomes $L - z_{bm1}$, where L is the channel length as indicated in Fig.3, and gradually goes to zero.

As discussed in previous works, e.g. [15, 17], the evaporation rate highly depends on the presence of the liquid corner films up to the channel entrance. The liquid is transported within the films from the main meniscus region up to the film tip region where it evaporates.

This transport induces the displacement of the bulk meniscus within the channel. Due to the so-called screening effects (see Section 4), evaporation is significantly more important in the channel entrance region than further inside the channel when the bulk meniscus has sufficiently receded into the channel. In other words, as reported in [28], evaporation from the main meniscus becomes rapidly negligible and evaporation actually occurs in the corner film tip region.

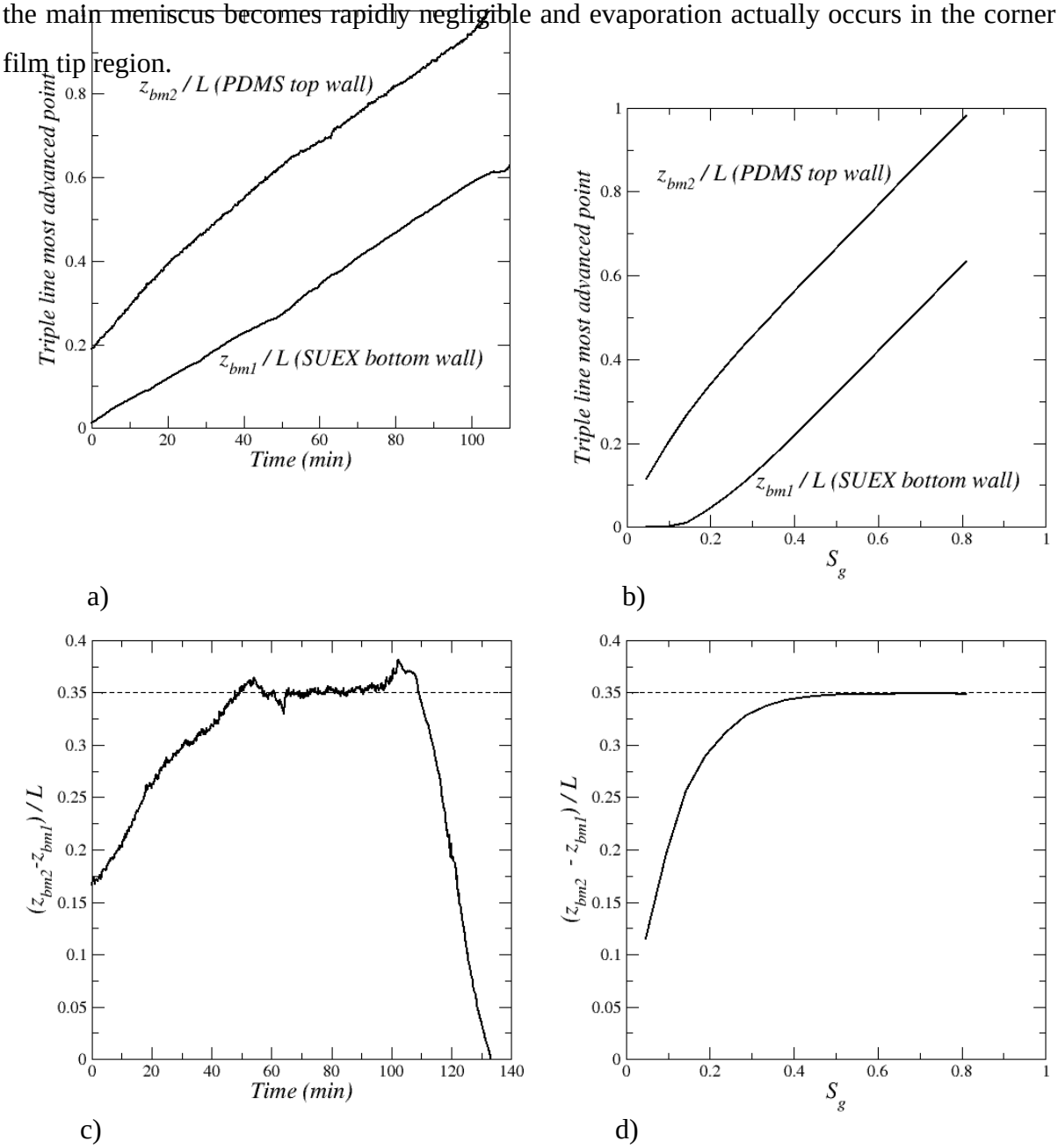

Fig. 7. (a) Experiment: Evolution of triple line most advanced point on SUEX bottom surface (z_{bm1} in Figs. 3 or 6) and on PDMS top surface (z_{bm2} in Figs. 3 or 6) for pure water, (b) Surface Evolver simulation: variation of triple line most advanced point on SUEX bottom surface and on PDMS top surface as a fraction of the volume fraction of gas in the channel, (c) Experiment: Evolution of the difference in the triple line most advanced point positions between PDMS top wall and SUEX bottom wall (i.e. $z_{bm2} - z_{bm1}$), (d) Surface Evolver

simulation.

Thus, the evaporation rate J is expected to decrease in the first period as the main meniscus recedes into the channel and to reach a constant value in the second period. The evaporation rate J and the liquid mass $m(t)$ within the channel (regardless of the liquid mass in the corner films for simplicity) are related by $J = -\frac{dm(t)}{dt} = -\rho_\ell \frac{dV_\ell}{dt}$ where ρ_ℓ is the liquid density and V_ℓ is the liquid volume limited by the main meniscus. The latter can be roughly expressed as $V_\ell \approx A\big(L - z_{bm2}(t)\big) + 0.5\,A\,(z_{bm2}(t) - z_{bm1}(t))$ as long as $z_{bm2}(t) < L$, where A is the channel cross-section surface area. As shown in Fig.7c, $z_{bm2}(t) - z_{bm1}(t) \approx constant$ for pure water in period 2. Thus, in this period, $\rho_\ell A \frac{dz_{bm2}(t)}{dt} = J$, which consistently leads to a linear variation of $z_{bm2}(t)$ with time (and thus also as regards $z_{bm1}(t)$ since $z_{bm2}(t) - z_{bm1}(t) \approx constant$) as J is expected to be constant due to the combination of the corner film and screening effects in this period. This is further discussed in Section 4.

As can be seen from Figs.7b and 7d, the simulation with Surface-Evolver leads to evolutions quite similar to those in the experiment. In the Surface Evolver simulations, there is no time scale and the parameter which is varied is the volume of gas present in the channel, or more precisely the gas saturation, i.e. the fraction S_g of the channel volume occupied by gas. As discussed before it is expected that S_g increases linearly with time since the evaporation is expected to be constant in the second period. For the sake of comparison between the experimental results and the Surface Evolver simulations (SES), the SES results have thus been plotted as a function of S_g in Figs. 7. The comparison between the SES and the experimental result in Figs. 7c and 7d indicates that the capillary forces control the shape of the liquid-gas interface in the case of the pure water experiment.

3.2 Evaporation kinetics (with particles)

The evolution of triple line most advanced points on SUEX bottom wall and PDMS top wall in the presence of particles is shown in Fig.8. Note that the initial filling of channel by the liquid phase, i.e. the initial liquid saturation, varies from one experiment to the other. For this reason, the following procedure was used to set a common time in all the experiments. Concerning Fig. 8a, the triple line on SUEX bottom wall observed in the first recorded image in the experiments was the most advanced inside the channel for the concentration 10^{-4} g/mL. Let label the experiments from 1 to 4 in order of increasing concentration. This position

max(z_{bm1-i}) was thus selected to set a common time for the four experiments. The time when this position is reached in each experiment is denoted by t_i. Thus t_4 = 0 for C = 10^{-4} g/mL. Then the time in the other experiments was shifted as $t_{newi} = t + (\max(t_i) - t_i)$. As a result of the time shift, the position max(z_{bm1-i}) is reached at the same time in the four experiments. Similarly, for Fig. 8b, the triple line on the PDMS wall observed in the first recorded image in the experiments was also the most advanced for the concentration 10^{-4} g/mL. The corresponding position was thus selected to set a common time for the four experiments in the same way. As can be seen from Fig.8, the triple line displacement is slower in the presence of particles both on PDMS top wall and SUEX bottom wall with an impact of the particles more marked as regards the triple line displacement on the bottom SUEX wall.

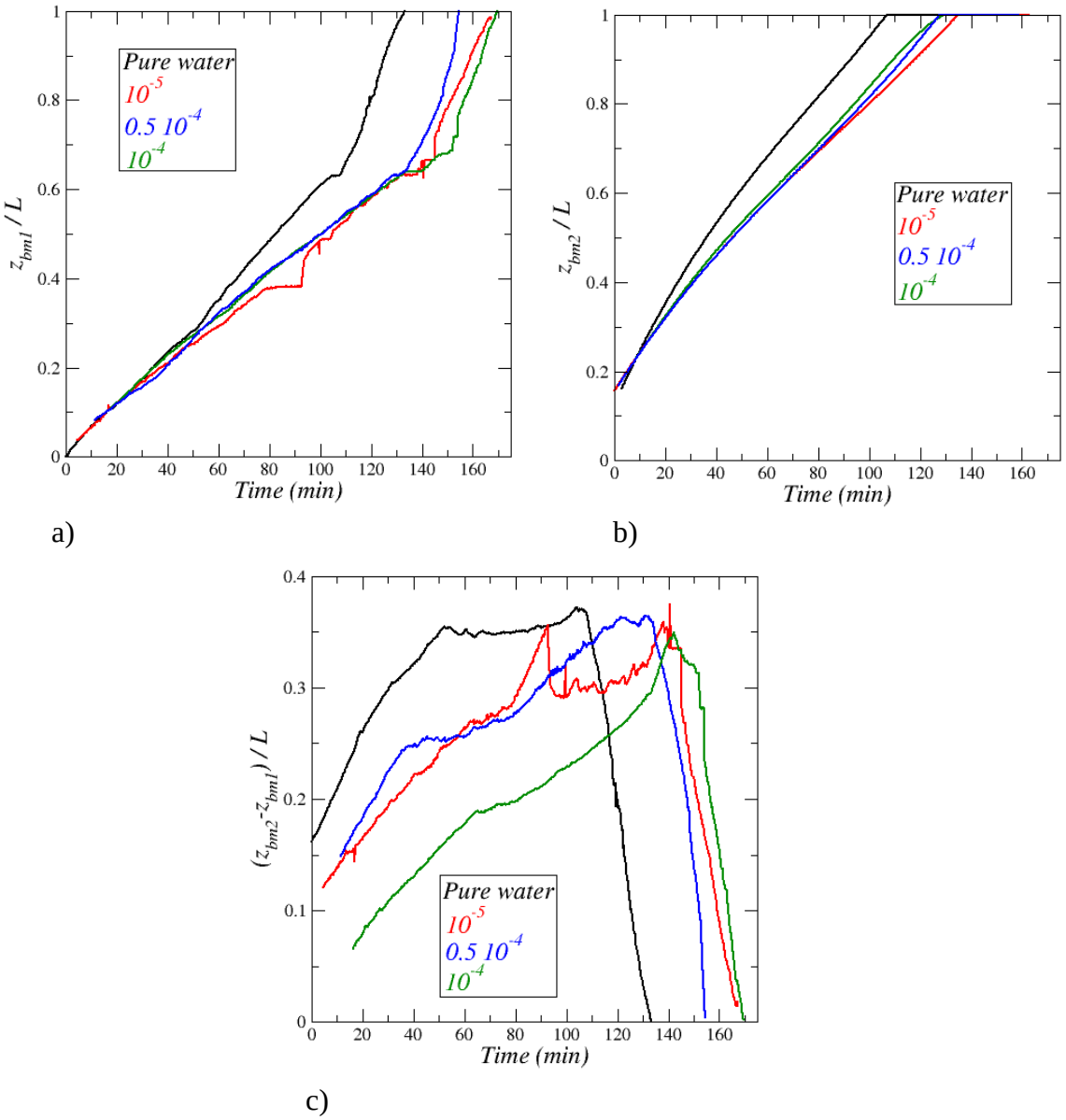

Fig. 8. (a) Evolution of triple line most advanced point on SUEX bottom surface (z_{bm1} in

Fig.3), (b) and PDMS top surface (z_{bm2} in Fig.3). **(**c**)** Experiment: Evolution of the difference in the triple line most advanced point positions between PDMS top wall and SUEX bottom wall (i.e. $z_{bm2} - z_{bm1}$) for the various concentrations in particles.

However, there is no clear difference on the results between the three particle concentrations. Based on a previous work on evaporation in the presence of colloidal particles from a granular porous medium [4], one could expect that the higher the concentration, the slower is the evaporation. However, as discussed in Section 5, the mechanism leading to the reduced evaporation, i.e. the film thinning, is different from the one considered in [4]. Figs. 5 and 6 indicate that the greater the concentration, the thinner is the film. However, this impact on the film thickness is too weak to impart a noticeable variation in the evaporation rate between the three particle concentrations tested. It can also be noticed that the evolution after t = 130 min in Fig.8a is not monotonic with the concentration.

As depicted in Fig.8c, an interesting difference can be observed between the pure water case and the case with particles when the difference $z_{bm2} - z_{bm1}$ between the triple line most advanced positions is plotted as a function of time (using the same procedure for setting a common time as for Fig. 8a). Note that z_{bm2} is set equal to the channel length L once the triple line on the PDMS top channel wall has reached the channel end.

This difference reaches a plateau in the case of the pure water experiment whereas it keeps increasing in the presence of particles. Also, this difference in the presence of particles is smaller than for pure water when the triple line on the PDMS top wall has not reached the channel end.

A peak can be observed in Fig.8c for the concentration 10^{-5} g/mL when t is the range [80 - 100] minutes. In fact, the triple line on the SUEX bottom gets pinned for a while due to a local accumulation of particles in the centre of the bottom wall whereas the triple line on the PDMS continues to move. As a result, the distance $z_{bm2} - z_{bm1}$ increases faster than for the other concentrations. When the triple line depinning occurs the triple line on the bottom SUEX wall moves rapidly toward a new capillary equilibrium. This is an illustration of a stick–slip phenomenon [24] explaining here the peak in the curve when t ~ 80 – 100 min. Similar stick-slip phenomena are observed for the other concentrations but the triple line remains stuck for less time than in the case of the peak in Fig.8c for the concentration 10^{-5} g/mL. Also, it can be observed from the movies that the stick-slip phenomena occur earlier for the smaller concentration (10^{-5} g/mL) than for the largest one (10^{-4} g/mL). Typically, when the main meniscus is in the last third of the channel for the concentration 10^{-4} g/mL

whereas the phenomenon can be observed over the last two third of the channel for the concentration 10^{-5} g/mL. The situation for the intermediate concentration (0.5×10^{-4} g/mL) is closer to concentration 10^{-5} g/mL than 10^{-4} g/mL. The fact that the stick-slip phenomenon becomes visible after a while can be explained by the fact that it takes some time for the particles to accumulate at and in the vicinity of the triple line. However, based on this argument, the stick-slip phenomenon should be expected to be observed earlier for the largest concentration whereas the contrary is observed. This remains to be explained. It can be also noticed that the stick-slip phenomenon can be observed both along the triple line region corresponding to the corner films and along the region corresponding to the main meniscus.

3.3 Final deposit

The final distribution of deposited particles after full evaporation is illustrated in Fig. 9. Very limited deposition occurred on the PDMS top plate. The deposits essentially formed on the SUEX walls. As shown in Fig.9, two main regions of deposited particles can be distinguished. The region where corner liquid films were present and the left and bottom corners at the junction between the channel bottom and the end wall.

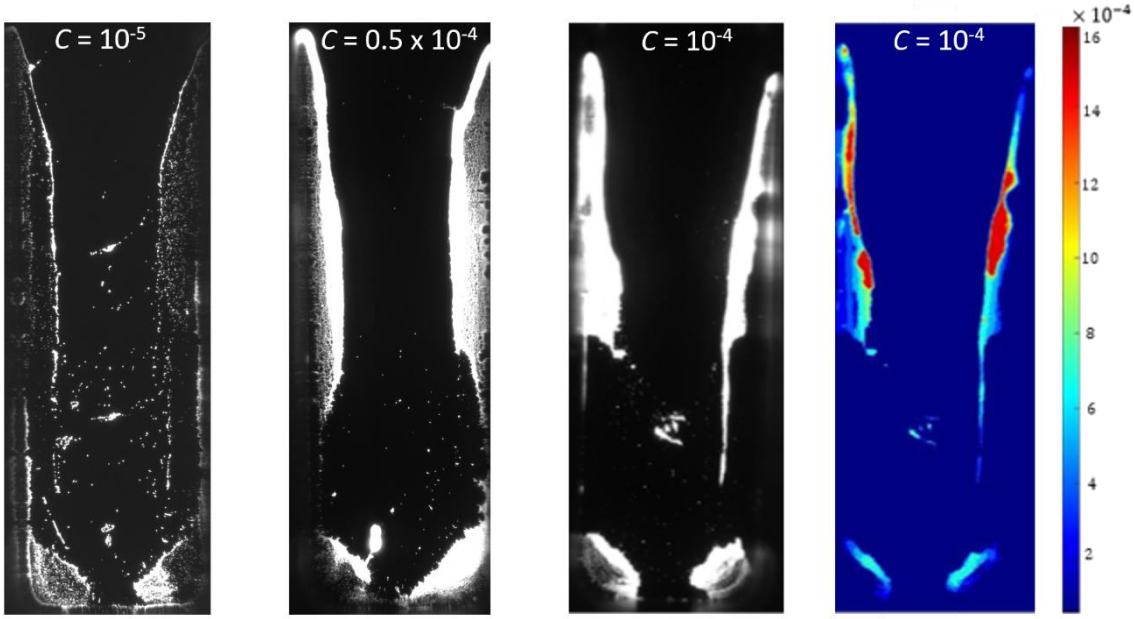

Fig. 9. Spatial distribution of deposited particles at the end of experiment after full evaporation. The preferential zones of particle deposition are in bright. The false color image on the right shows a more detailed information on the deposited particle distribution for the highest concentration tested.

The latter are fully consistent with the evolution of the liquid gas distribution toward the end of evaporation computed with Surface-Evolver (Fig.10), showing the formation of two liquid wedges in the corresponding corners. It is recalled that the Surface Evolver simulation corresponds to the case of pure water (no particles). The possible effect of the presence of the particles is roughly addressed in Fig.10 by considering two values of contact angle on the SUEX wall (the contact angle on the PDMS wall imposed in these simulations is 104°). For both values, above and below the critical contact angle of 45°, the terminal wedge effect is obtained.

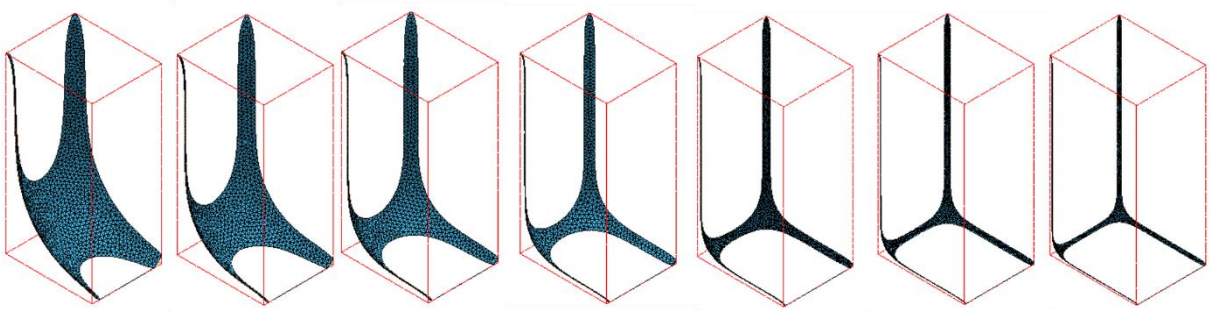

$\theta_{SUEX} = 30°$

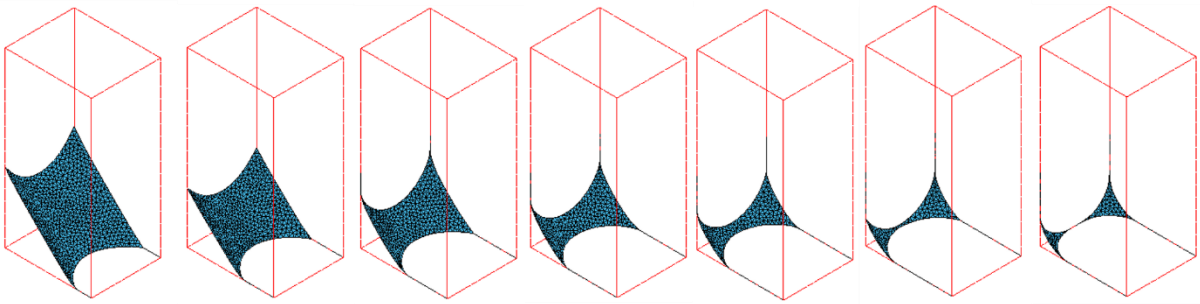

$\theta_{SUEX} = 50°$

Fig. 10. Final liquid distribution in the composite channel as computed by Surface Evolver for two values of contact angle on the SUEX walls.

The greater the concentration, the greater is the brightness of the deposits in Fig.9, indicating, as expected, a greater accumulation of deposited particles with an increasing initial particles concentration. More details can be seen for the highest concentration (C = 10^{-4} g/mL) in the image in false color in Fig.9. To obtain this image, the calibration curve has been used to convert the light intensity into particle concentration (considered as an indicator of particle accumulation since the particles are not in a suspension in this image whereas the calibration curve was established with particles in suspension). This image indicates a greater particle accumulation in the films compared to the end wedge region. Also, this image indicates than the particle deposit in the films is heterogeneous with more deposited particles in the upper

region of the films and in the vicinity of the triple line.

4 Impact of corner film thickness on evaporation rate

Numerical simulations are performed to evaluate the impact of film thickness on evaporation rate. The simulations correspond to the films illustrated in Fig.4, namely pure water for three values of contact angle on SUEX (20°, 30°, 40°). The gas-liquid interface in the channel (as illustrated in Fig.3) is computed using Surface Evolver [20]. Then the result is imported in the commercial software COMSOL Multiphysics considering the computational domain illustrated in Fig.11.

Based on a previous work [29], the size of the hemisphere shown in Fig.11a is selected so as to be sufficiently large for the results to be independent of its size. The diffusion equation is solved in the channel (gas region) and within the gas region in the hemisphere imposing a dimensionless vapor partial pressure of 1 on the liquid-gas interface and zero on the hemisphere limiting surface. Zero flux condition is imposed on the solid walls. In fact, the vapor partial pressure gradients are significant only in a small region of the computational domain in the vicinity of the channel entrance. This is further shown in Fig.11c illustrating the so-called screening effect, i.e. the fact that the vapor partial pressure gradients vanish inside the channel due to the presence of the corner films.

This gives the variation of the evaporation rate depicted in Fig.11d. As can be seen, the evaporation rate when the film is established (as depicted in Fig.5) is little less than half that of the full liquid channel (inset in Fig.11d). When the contact angle on SUEX is varied from 20° to 40°, the film thickness (defined in Fig.11d and made dimensionless using the channel width) varies from about 0.22 to 0.06, which is comparable to the variation depicted in Fig.6 between the case of pure water and that in the presence of particles. This variation corresponds to a reduction of about 20% in the evaporation rate (Fig.11d) and illustrates the strong impact of the corner film thickness on the evaporation rate. From the estimate of the evaporation rate in the experiment $J \approx \rho_\ell A \frac{dz_{bm1}(t)}{dt}$, this 20% variation is fully consistent with the mean variation in the slope, i.e. $\frac{1}{L}\frac{dz_{bm1}}{dt}$, in Fig. 8 (before the position 0.6 is reached) between the case of pure water and that with particles (the slope ratio between both cases is about 0.81).

In conclusion, the presence of the particles makes the corner films thinner in the channel

entrance region, which is the region of most active evaporation in the channel, and this reduces the evaporation compared to the case of pure water, which corresponds to the thickest films.

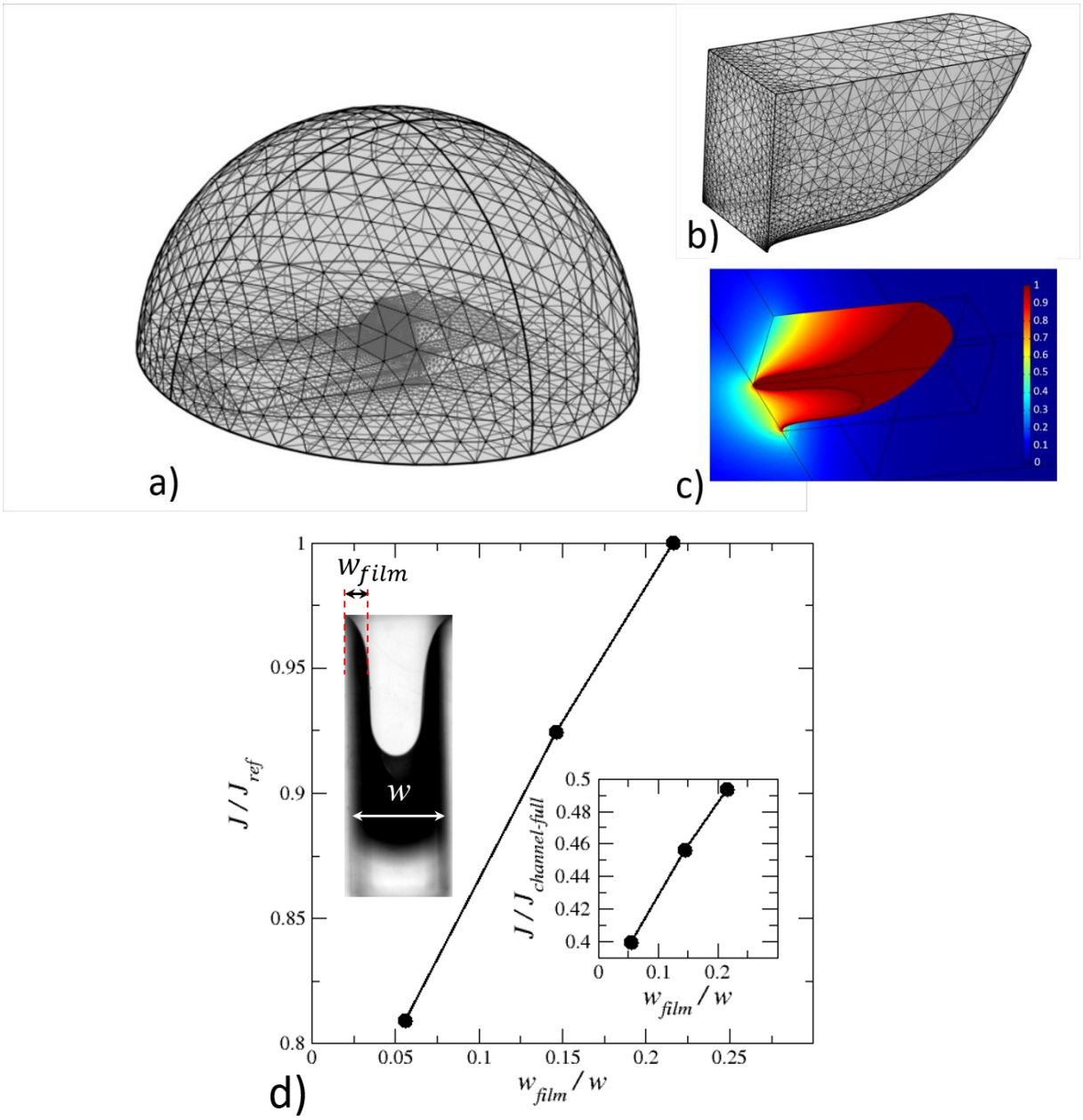

Fig.11. Impact of film thickness on evaporation rate from the channel from numerical simulations. a) computational domain, b) computational domain in the channel (gas region), c) illustration of normalized vapor partial pressure field (dimensionless) in the channel, d) Variation of evaporation rate as a function of film thickness (in the inset the evaporation rate is normalized by the evaporation rate from the fully liquid saturated channel).

.5. On the accumulation of particles in the films and the film thinning effect

5.1 Particle convective transport is dominant in the films

The preferential accumulation of particles in the corner liquid films is consistent with a dominant convective transport of the particles within the films. This can be supported from the estimate of the Péclet number characterizing the competition between the diffusive and convective transports in the films [30]. The latter is expressed as $Pe = \frac{Ul}{D}$, where U is a characteristic liquid velocity in the films, l is the length of the films and D is the particle diffusion coefficient. The latter can be estimated using the Stokes-Einstein law. For 1 µm diameter particles, this gives $D \sim 10^{-13}$ m^2/s. The velocity in the films can be estimated as $U = \frac{1}{A_c}\frac{J}{2\rho_\ell}$ [17], where J is the evaporation rate and A_c is the cross-section surface area of a corner film. For simplicity, the latter is estimated for the case of pure water and the contact angle of 30° (Fig.4) from the formula given in [17] (and also in the Supplementary material of the present article). As mentioned in Section 3.1, the evaporation rate can be estimated as $J = \rho_\ell A \frac{dz_{bm2}(t)}{dt}$. Application for $l = L/2$ gives $Pe \approx$ O(10^5), which corresponds to a highly dominant convective transport of the particles within the films. It is well known, e.g. [13], that a large Péclet number corresponds to the preferential accumulation of the particles at the evaporation front. Thus, here, one could expect that the particles accumulate along the film liquid-gas interface. This is roughly what can be seen from Fig.9. However, as illustrated in the image in false-color in Fig.9, the greater accumulation at the end of the evaporation is not at the film top but deeper inside the channel. This heterogeneous distribution is in part due to what happens in the final step when the films disconnect from the channel end and fully evaporate. However, the inspection of the movies suggests a relatively complex particle dynamics in the films during evaporation with possible particle recirculation effects within the films. These recirculation effects should also play a role in the particle distribution within the films and would deserve to be explored in details in future works.

5.2 Accumulation of particles and particle compact packing in the corner films

In [1] and [4], the reduced evaporation rate observed in the presence of particles was

attributed to the formation of a compact packing of particles and the formation of a dried zone in the accumulation zone of particles. As in a classical drying problem in porous media, e.g. [31], the presence of the evaporation front at the boundary of the particle packing depends on the competition between viscous and capillary effects. When the pressure drop in the liquid phase due to the viscous flow induced by the evaporation process is too large the capillary effects are not sufficient to maintain the front at the particle packing boundary and the front recedes into the packing. This leads to the formation of a dry zone introducing an additional mass transfer resistance. A similar mechanism of particle accumulation and receding front was observed in corner films in a single channel in [32]. Although assuming completely dry the zone ahead of the front did not lead to results fully consistent with the experiment, the impact of the particles on the evaporation rate was quite noticeable.

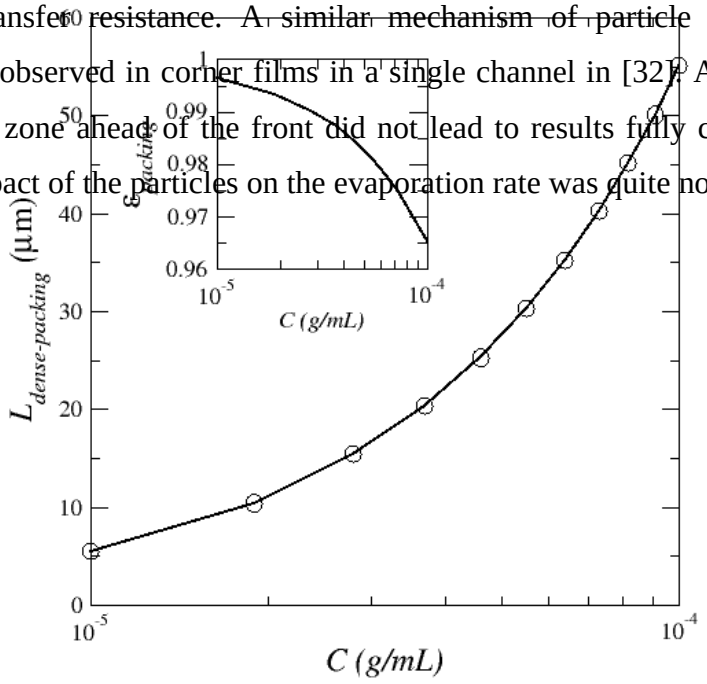

Fig.12. Size of a compact particle packing in the corner films made of all particles introduced in the channel. The inset shows the particle volume fraction in the corner films assuming a uniform distribution of all the particles in the corner films for z_{bm1}=1mm.

Thus, the question arises as to whether a similar phenomenon can contribute to explain the reduced evaporation observed in our experiments. A simple argument indicating that the situation is different in the case of our experiments consists in evaluating the volume fraction of particles in the corner films. The total number of particles in the channel is $N_p = V_{ch}C/m_p$, where V_{ch} is the channel volume (assuming here that the channel is fully filled by

the solution initially), C is the particle concentration and m_p is the mass of one particle. Let's assume a contact angle of 30°, a film thickness of 80 µm (Fig.6), a film extent z_{bm1} of 1 mm and that all the particles are uniformly distributed within the two corner films. Then the particle volume fraction in the films is $\varepsilon_s = (N_p/2)\, V_p/A_c/z_{bm1}$, where V_p is the volume of one particle and A_c is the film cross-section surface area (see the Supplementary material for details on how A_c can be estimated). This gives the results shown in Fig.12 (inset) indicating that the particle volume fraction ε_s is quite low.

In other words, contrary to the situation analyzed in [1] or [32], a compact packing of particles (corresponding to $\varepsilon = 1 - \varepsilon_s \approx 0.37$) cannot form over a significant region of the corner films.

To discuss further this aspect, suppose the particles are all in the tip region of the corner films and form a compact packing. The length L_{cp} of this compact zone within the corner film can be estimated from the equation $L_{cp}\,(1-\varepsilon)A_c = (N_p/2)V_p$, where $\varepsilon \approx 0.37$ (compact packing). This gives the results shown in Fig.12. As can be seen, the length of such a packing is on the order of a few tens of micrometers. This is too small to expect the dry zone formation to form and to affect the evaporation rate.

Consistently with the observations a compact arrangement of the particles can thus be expected only in the vicinity of the triple line during the evaporation process in the channel.

Also, it can be noted that the particles are too large in our experiments to expect an impact of the Kelvin effect on the evaporation rate [2].

Consistently with the results presented in Section 4, the conclusion is therefore that the reduced evaporation observed in our experiments in the presence of particles is due to the film thinning and not to the formation of a dry zone in the corner film region or the Kelvin effect. Then, the question remains why does the presence of the particles lead to thinner corner films compared to pure water? This is discussed in the next sub-section.

Nevertheless, the comparison with the results reported in [32] suggests to distinguish at least two regimes. The situation studied in [32] would correspond to a "high" concentration regime where the particles are sufficiently numerous for forming a compact packing in a significant region of the corner films whereas the situation considered in our experiments would correspond to a "low" concentration regime where the number of particles in the corner films is much lower and the compact packing, if any, is limited to the vicinity of the triple lines and the liquid –gas interface.

5.3 On the effect of particles on corner films

From previous works, e.g. [15, 17, 28], it is known that the corner film thickness depends on the contact angle and the competition between the capillary and viscous forces (gravity effects being negligible in the present experiment). As mentioned before, the contact angle must be lower than a critical value θ_c for the corner films to develop (θ_c = 45° for right angle corner, [27]). The lower the contact angle below θ_c, the thicker the corner films are, all other factors being equal.

To explain the film thinning seen in the experiments with particles, a first possibility could be the effect of particles on surface tension. As reported in [33], the presence of particles can reduce the surface tension. Let's consider that the surface tension varies with the particle concentration. The quasi-static corner meniscus curvature radius distribution is given by

$$\frac{\gamma(z)}{R} = \frac{\gamma(z_0)}{R_{th}} \tag{1}$$

where R is the corner meniscus curvature radius (see Fig.A1 in the Supplementary material) and R_{th} is the corner film curvature radius at the junction with the bulk meniscus (see Supplementary material). This leads to

$$w_{film}(z) = (cos\theta - sin\,\theta)R_{th}\frac{\gamma(z)}{\gamma(z_0)} \tag{2}$$

where w_{film} is the film thickness (Fig.5 and Fig.A1 in the Supplementary material).

The maximum surface tension variation in [33] due to particles is from 71 × 10^{-3} N/m to about 67 × 10^{-3} N/m. According to Eq.(2), $\frac{w_{film}(z)}{w_{film}(z_0)} = \frac{\gamma(z)}{\gamma(z_0)}$. Thus, the maximum film thickness variation due to this effect can be expected to be $\frac{w_{film}(z)}{w_{film}(z_0)} = \frac{\gamma(z)}{\gamma(z_0)} \approx 0.94$. Based on the results shown in Figs. 5 and 6, this effect is too weak to explain the corner film thinning observed in the experiment. Furthermore, it is likely that the decrease in the surface tension is partly compensated by a decrease in the contact angle.

Another possibility lies in the effect of the particles on the suspension viscosity. Since evaporation induces a liquid flow in the films, this liquid flow induces a viscous pressure drop along the film. When this viscous pressure drop is negligible compared to the pressure jump, i.e. the capillary pressure, at the liquid-vapor interface, the film thickness does not vary along the channel except in the channel entrance region. This is the situation in the pure water experiment (Fig.3). When the viscous pressure drop is not negligible, the capillary pressure varies along the corner films. This induces the spatial variation of the film thickness, which increases along the corner from the channel entrance. Since the film thickness

increases along the corners in Fig.5, it is tempting to consider that the effect of the particles is to increase the suspension viscosity at a sufficient level for impacting the film thickness.

To evaluate the viscous pressure drop required to obtain a noticeable thinning of the film, the model presented in [17] is used. The details are presented in the Supplementary material (SM). As illustrated in Fig.A2 in SM, it is found that the viscosity must be about three orders of magnitude greater than the viscosity of pure water for the corner film thickness variation along the channel to be comparable to that seen in the experiment in the presence of particle (Figs.5 and 6). However, the data reported in [34] indicates that the maximum increase in the viscosity due to the presence of particles is by about a factor 100, thus an order of magnitude lower than the value estimated for obtaining a film thinning comparable to the experiment. Also, the film thickness at a given location decreases with time when the film thinning is due to viscous effects. This is not what is seen in the experiments in the presence of particles since the film shape at a given location does not vary with time once formed (except at the very end of the experiment when the liquid totally disappears and on the few places where the stick-slip phenomenon mentioned in Section 3.2 and also discussed below occurs). Also the particle concentration in the films is actually quite low (as discussed in Section 5.2). Thus the impact of particles on the suspension viscosity is in fact negligible. The corner film thinning in the presence of the particles cannot therefore be attributed to the increase in the suspension viscosity due to the presence of the particles.

Finally, as illustrated in Fig.5, the conclusion is that the film shape is essentially affected by the local accumulation of particles in the vicinity of the triple line. Once the particle concentration at the triple line is sufficiently high, particles locally form a compact packing and the triple line gets pinned and this leads to the film thinning illustrated in Fig.5. However, the details on the complex dynamics of pinning and local packing formation leading to the corner film shapes shown in Fig.5 remain to be unraveled. For instance, as mentioned before, the inspection of the movies does indicate some occasional stick-slip motion of the triple line in the presence of particles. Perhaps, a detailed analysis of this stick-slip effect, e.g. [24], might help better understand the capillary film thinning phenomenon in the presence of particles. Also, it has been reported that the wettability of the particles has an impact on the motion of the triple line, e.g. [24]. Repeating the experiments changing the particle wettability could be insightful.

5 Conclusions

From a combination of visualization experiments and numerical simulations, this work has demonstrated that the presence of colloidal particles reduces evaporation from a single channel compared to the situation in the absence of particles. Consistently with previous works [15-18] showing the strong impact of liquid corner films on evaporation, this work shows that the evaporation reduction effect is due to the effect of particles on the corner films. The particle accumulation in the corner liquid films modifies the dynamics of the corner films. The latter are thinner compared to pure water, which in turn reduces the evaporation rate [18]. In addition to the corner films, the experiments show that particles also tend to accumulate in the regions of the channel which are the last ones to empty. These correspond to the two hydrophilic corners at the channel closed end in the presented experiments.

In complement with previous works showing an evaporation reduction effect due to the particles at the scale of a porous medium [4] or a single channel [1], [2], [32], the present study thus sheds light on an evaporation reduction mechanism at pore scale, i.e. the corner film thinning effect, different from the ones considered in these previous works where the evaporation reduction was related to the formation of a compact packing of particles inducing the receding of the evaporation front in the porous medium or the channel. In that respect, the present study suggests to distinguish the low particle concentration regime explored in the present article from the higher concentration regime considered in the above-mentioned previous works. Together with these works, it is thus expected that the insights gained from the simple geometry considered in the current work will be useful for the understanding and modeling of evaporation in the significantly more complex case of evaporation in porous media in the presence of particles [4, 10, 12].

In line with a previous work [22], the study also shows that the knowledge of the “fresh” value of the contact angle is not sufficient to infer whether or not corner films can develop since the contact angle value can decrease as the result of evaporation and the pinning of the triple line. In the case of the reported experiments, the contact angle fresh value on the hydrophilic material was of on the order of 70°, thus not compatible with the formation of liquid films in right corners, whereas significant corner film effects could in fact be observed. The latter corresponded to a contact angle value of about 30°, consistent with the contact angle evolution measured in a separate droplet evaporation experiment.

A natural next step will be to investigate the effect of particles on evaporation in networks of interconnected channels [19, 35-37] as microfluidic tools for scale bridging between the single channel and porous media.

CRediT authorship contribution statement

Elisa Ghiringhelli: Experiments, Data analysis, Image processing, Writing – original draft. **Manuel Marcoux**: Experiments Conceptualization and Supervision, Editing. **Sandrine Geoffroy**: Numerical simulations. **Marc Prat:** Conceptualization, Investigation, Modelling, Writing – review & editing.

Declaration of Competing Interest

The authors declare that they have no known competing financial interests or personal relationships that could have appeared to influence the work reported in this paper.

Acknowledgements: Authors are grateful to Julien Lefort (IMFT) and Sebastien Cazin (IMFT) for the help during the experiments.

References

1. E. R. Dufresne, E. I. Corwin, N. A. Greenblatt, J. Ashmore, D. Y. Wang, A. D. Dinsmore, J. X. Cheng, X. S. Xie, J. W. Hutchinson, D. A. Weitz, Flow and fracture in drying nanoparticle suspensions, Phys. Rev. Lett. 91 (2003) 224501.
2. P. Lidon, J.-B. Salmon, Dynamics of unidirectional drying of colloidal dispersions, Soft Matter 10 (2014) 4151–4161
3. O. D. Velev, S. Gupta, Materials Fabricated by Micro-and Nanoparticle Assembly–The Challenging Path from Science to Engineering, Adv. Mater. 21(19) (2009) 1897-1905.
4. E. Keita, P. Faure, S. Rodts, P. Coussot, MRI evidence for a receding-front effect in drying porous media, Phys. Rev. E 87 (2013) 062303.
5. E. Michel, S. Majdalani, L. Di-Pietro, How differential capillary stresses promote particle mobilization in macroporous soils: A novel conceptual model, Vadose Zone J. 9 (2) (2010) 307–316.
6. B. Alramahi, K. Alshibli, D. Fratta, Effect of fine particle migration on the small-strain stiffness of unsaturated soils, Journal of Geotechnical and Geoenvironmental Engineering, Vol. 136 (4) (2010) 620-628.
7. H. Ito, K. Abe, M. Ishida, A. Nakano, T. Maeda, T. Munakata, H. Nakajima, T. Kitahara Effect of through-plane distribution of polytetrafluoroethylene in carbon paper on in-plane gas permeability, Journal of Power Sources 248 (2014) 822-830.

8. T. Brunschwiler, J. Zürcher, L. Del Carro, G. Schlottig, B. Burg, S. Zimmermann, U. Zschenderlein, B.Wunderle, F. Schindler-Saefkow, R. Stässle, Review on percolating and neck-based underfills for three-dimensional chip stacks. J. Electron. Packag. 138(4) (2016) 041009.
9. P. Bacchin, D. Brutin, A. Davaille, E. Di Giuseppe, X. D. Chen, I. Gergianakis, F. Giorgiutti-Dauphiné, L. Goehring, Y. Hallez, R. Heyd, R. Jeantet, C. Le Floch-Fouéré, M. Meireles, E. Mittelstaedt, C. Nicloux, L. Pauchard, M.-L. Saboungi. Drying colloidal systems: Laboratory models for a wide range of applications, The European Physical Journal E 41 (2018) 94.
10. E Keita, T.E. Kodger, P. Faure, S. Rodts, D.A. Weitz, P. Coussot. Water retention against drying with soft-particle suspensions in porous media, Physical Review E 94 (3) (2016) 033104.
11. E Keita, Particle Deposition in Drying Porous Media, Materials 14 (18) (2021) 512012.
12. F. Qin, A. Mazloomi Moqaddam, Q. Kang, D. Derome, J. Carmeliet, LBM simulation of self-assembly of clogging structures by evaporation of colloidal suspension in 2D porous media, Transport in Porous Media 128 (2019) 929–943.
13. H.P. Huinink, L. Pel, M.A.J. Michels, How ions distribute in a drying porous medium: A simple model, Physics of Fluids 14 (2002) 1389-1395.
14. H. Eloukabi, N. Sghaier, S. Ben Nasrallah, M. Prat. Experimental study of the effect of sodium chloride on drying of porous media: the crusty-patchy efflorescence transition. Int. J. of Heat and Mass Tr. 56 (2013) 80-93.
15. F. Chauvet, P. Duru, S. Geoffroy, M. Prat, Three periods of drying of a single square capillary tube, Phys. Rev. Lett. 103 (2009) 124502.
16. A. G. Yiotis, A. G. Boudouvis, A. K. Stubos, I. N. Tsimpanogiannis, Y. C. Yortsos, Effect of liquid films on the drying of porous media, AiChE J. 50 (11) (2004) 2721-2737.
17. M.Prat, On the influence of pore shape, contact angle and film flows on drying of capillary porous media, Int. J. of Heat and Mass Tr., 50 (2007)1455-1468.
18. A.G. Yiotis, D. Salin, E.S. Tajer, Y.C. Yortsos, Drying in porous media with gravity-stabilized fronts: Experimental results, Physical Review E 86 (2012) 026310.
19. J.J. Zhao, Y.Y. Duan, X.D. Wang, B.X. Wang. Effect of nanofluids on thin film evaporation in microchannels. J. of Nanoparticle Research, 13(10) (2011) 5033-5047.
20. J.B.Laurindo et M.Prat. Numerical and experimental network study of evaporation in capillary porous media. Drying rates, Chem.Eng.Sci. 53(12) (1998) 2257-2269.
21. K.A. Brakke. The surface evolver. Exp. Math. 1 (2) (1992) 141–165.

22. A. Mata, A.J. Fleischman, S. Roy. Characterization of polydimethylsiloxane (PDMS) properties for biomedical micro/nanosystems. Biomedical Microdevices 7 (2005) 281–293.
23. H. Mishra, A. M. Schrader, D.W. Lee, A. Gallo, Jr., S.-Y. Chen, Y. Kaufman, S. Das, and J. N. Israelachvili, Time-Dependent wetting behavior of PDMS surfaces with bioinspired, hierarchical structures, ACS Appl. Mater. Interfaces 8 (12) (2016) 8168–8174.
24. D.-O. Kim, M. Pack, A. Rokoni, P. Kaneelil, Y. Sun, The effect of particle wettability on the stick-slip motion of the contact line, Soft Matter 14 (2018) 9599
25. S.Geoffroy, F.Plouraboué, M.Prat, O.Amyot, Quasi-static liquid–air drainage in narrow channels with variations in the gap, J. of Coll. Int. Sci. 294 (2006) 165-175.
26. E. Keita, S. A. Koehler, P. Faure, D. A. Weitz, P. Coussot, Drying kinetics driven by the shape of the air/water interface in a capillary channel, The European Physical Journal 39 (2016) 23.
27. P. Concus, R. Finn. On the behavior of a capillary surface in a wedge. Proceedings of the National Academy of Sciences 63 (1969) 292-299.
28. F.Chauvet, P.Duru, M. Prat, Depinning of evaporating liquid films in square capillary tubes: influence of corners roundness, Phys. of Fluids 22 (2010) 112113.
29. S.Beyhaghi, S.Geoffroy, M. Prat, K. M. Pillai, Wicking and Evaporation of Liquids in Porous Wicks: A Simple Analytical Approach to Optimization. AIChE J., 60 (5) (2014) 1930 – 1940.
30. B.Camassel, N.Sghaier, M.Prat, S.Ben Nasrallah, Ions transport during evaporation in capillary tubes of polygonal cross section. Chem. Eng. Sci., 60 (2005) 815-826.
31. M.Prat, Recent advances in pore-scale models for drying of porous media, Chem. Eng. J., 86 (2002), 153-164.
32. M. D. Seck, E. Keita, P. Coussot, Some observations on the impact of a low-solubility ionic solution on drying characteristics of a model porous medium. Transport in Porous Media, 128 (2019) 915–928.
33. L.Dong, D.Johnson, Surface Tension of Charge-Stabilized Colloidal Suspensions at the Water-Air Interface, Langmuir 19 (2003) 10205-10209.
34. D. G Thomas, Transport characteristics of suspension: VIII. A note on the viscosity of Newtonian suspensions of uniform spherical particles, J. of Colloid Science 20 (3) (1965) 267-277.

35. N. Vorhauer, Y. Wang, A. Karaghani, E. Tsotsas, M. Prat, Drying with formation of capillary rings in a model porous medium SI Drying. Transport in Porous Media 110 (2015) 197-223.
36. P. Fantinel, O. Borgman, R. Holtzman, L. Goehring, Drying in a microfluidic chip: experiments and simulations. Scientific Reports 7 (2017) 15572.
37. R. Wu, T. Zhang, C.Ye, C. Y. Zhao, E. Tsotsas, A. Kharaghani, Pore network model of evaporation in porous media with continuous and discontinuous corner films. Phys. Rev. Fluids 5 (2020) 014307.

Graphical abstract

Evaporation in a channel of rectangular cross-section leads to the formation of corner liquid films

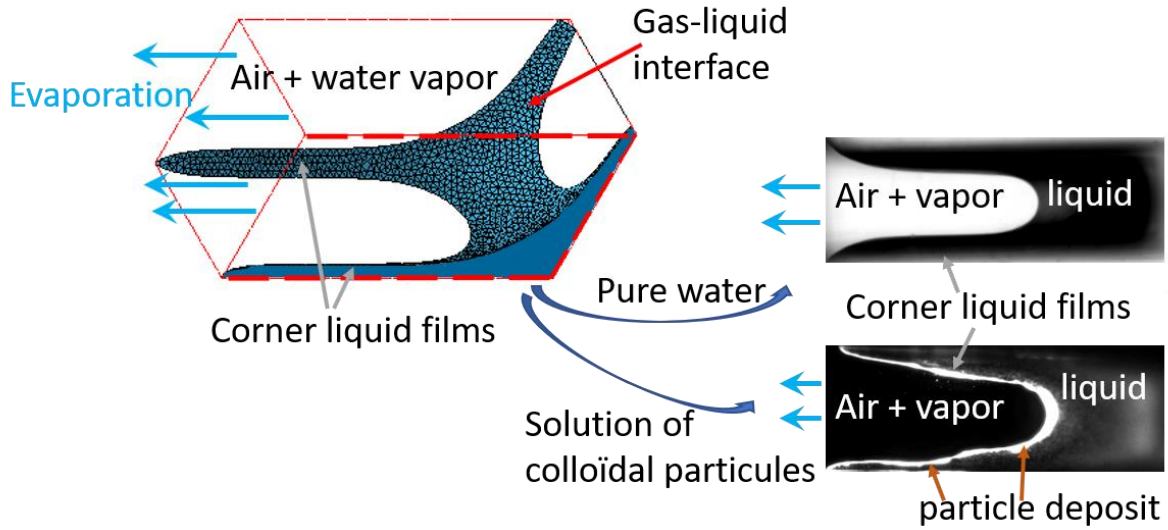

Preferential particle deposit in corner films induces film thinning and reduced evaporation compared to pure water